

Fabrication, characterisation and analytical modelling of gradient auxetic closed cell foams

DUNCAN, Olly <<http://orcid.org/0000-0001-9503-1464>>, ALDERSON, Andrew <<http://orcid.org/0000-0002-6281-2624>> and ALLEN, Tom <<http://orcid.org/0000-0003-4910-9149>>

Available from Sheffield Hallam University Research Archive (SHURA) at:

<https://shura.shu.ac.uk/28069/>

This document is the Accepted Version [AM]

Citation:

DUNCAN, Olly, ALDERSON, Andrew and ALLEN, Tom (2021). Fabrication, characterisation and analytical modelling of gradient auxetic closed cell foams. Smart Materials and Structures. [Article]

Copyright and re-use policy

See <http://shura.shu.ac.uk/information.html>

ACCEPTED MANUSCRIPT

Fabrication, characterisation and analytical modelling of gradient auxetic closed cell foams

To cite this article before publication: Olly Duncan *et al* 2021 *Smart Mater. Struct.* in press <https://doi.org/10.1088/1361-665X/abdc06>

Manuscript version: Accepted Manuscript

Accepted Manuscript is “the version of the article accepted for publication including all changes made as a result of the peer review process, and which may also include the addition to the article by IOP Publishing of a header, an article ID, a cover sheet and/or an ‘Accepted Manuscript’ watermark, but excluding any other editing, typesetting or other changes made by IOP Publishing and/or its licensors”

This Accepted Manuscript is © 2020 IOP Publishing Ltd.

During the embargo period (the 12 month period from the publication of the Version of Record of this article), the Accepted Manuscript is fully protected by copyright and cannot be reused or reposted elsewhere.

As the Version of Record of this article is going to be / has been published on a subscription basis, this Accepted Manuscript is available for reuse under a CC BY-NC-ND 3.0 licence after the 12 month embargo period.

After the embargo period, everyone is permitted to use copy and redistribute this article for non-commercial purposes only, provided that they adhere to all the terms of the licence <https://creativecommons.org/licenses/by-nc-nd/3.0>

Although reasonable endeavours have been taken to obtain all necessary permissions from third parties to include their copyrighted content within this article, their full citation and copyright line may not be present in this Accepted Manuscript version. Before using any content from this article, please refer to the Version of Record on IOPscience once published for full citation and copyright details, as permissions will likely be required. All third party content is fully copyright protected, unless specifically stated otherwise in the figure caption in the Version of Record.

View the [article online](#) for updates and enhancements.

Fabrication, characterisation and analytical modelling of gradient auxetic closed cell foams

Olly Duncan^{1*}, Andrew Alderson², Tom Allen¹

¹ *Department of Engineering, Faculty of Science & Engineering, Manchester Metropolitan University, John Dalton Building, Chester Street, Manchester M1 5GD, UK.*

² *Materials and Engineering Research Institute, Faculty of Science, Technology and Arts, Sheffield Hallam University, Howard Street, Sheffield S1 1WB UK.*

* Corresponding author (Email: O.Duncan@mmu.ac.uk)

Abstract

Auxetic (negative Poisson’s ratio) and gradient open cell foams have shown promise for their conformability and high impact energy absorption – useful in applications like protective equipment, footwear and prosthetics. Recent methods fabricated closed cell auxetic foam by steaming conventional closed cell foam. Methods developed herein control the cell structure of auxetic closed cell foam, to produce novel intentionally anisotropic and gradient auxetic closed cell foam. Pins passed through the foam constrained or stretched regions during steaming to further modify cell structure and impart gradients in cell structure, Young’s modulus and Poisson’s ratios. Fabricated foams had Poisson’s ratios between 1 and -1. Imparted Young’s moduli of 1 to 12 MPa were similar to foams used in footwear, prosthesis, helmets and other impact protection. The effect of changes to cell structure on Young’s moduli and Poisson’s ratio are explained by combining analytical models of auxetic open cell and conventional closed cell foam.

Keywords

negative Poisson’s ratio, gradient, foam, impact protection, steam processing

1. Introduction

Auxetic foam has a negative Poisson’s ratio (NPR; expanding transversely when stretched and contracting transversely when compressed) [1]. NPR can increase conformability [2,3], indentation resistance [4,5], impact energy abortion [6–8], vibration damping [9–11], acoustic [12–14] and thermal insulation [15,16] and shear modulus [17,18], while also causing biaxial expansion and domed curvature [19,20]. Auxetic open cell foams, with established fabrication

methods [1,21,22], have been proposed and tested for a range of applications, including in prosthetic devices [19,23], seating [24], footwear [25], vibration limiting gloves for use in construction [11], crash barriers and pads [24,26], sports helmets [27] and other personal protective equipment [8,26,28]. Most auxetic foam research focusses on open cell foam with Young's modulus below ~ 0.2 MPa [29,30]. A recent study produced low porosity open cell foam sheets with planar NPR in tension, and through thickness Young's moduli up to 25 MPa [31]. Personal protective equipment generally uses porous closed cell foam, containing trapped gas or air to increase the stiffness provided by the foam cell structure to between 1 and 20 MPa [32–34]. Without established methods to fabricate porous auxetic foams with desirable stiffness, products containing auxetic foams are not common.

Typical auxetic open cell foam fabrications first compress conventional thermo-plastic open cell foam, buckling cell ribs to impart a re-entrant like cell structure, which is commonly associated with NPR [1,21,22]. Heating and cooling cycles can then fix the imposed structure over time, so these fabrications are known as thermo-mechanical fabrications [1,21,35]. Solvents or gases can also be used as softening agents [22,36,37]. Anisotropic auxetic open cell foams can be made by applying different levels of compression in different directions [6,31,38]. Thermo-forming with curved moulds can also produce curved auxetic open cell foam [39]. Thermo-forming recently produced foam sheets with tensile NPR in both planar directions. The foam was highly compressed through thickness during thermo-forming, reducing through thickness porosity while imparting Young's modulus up to 25 MPa and positive compressive Poisson's ratio [31].

Gradient foams have different cell structures, Young's moduli and Poisson's ratio in pre-defined regions, and gradients can be discrete or continuous [19,23,40]. During open cell auxetic gradient foam fabrications, compression can be controlled, and hence varied, by passing pins through the foam sample, or by using a foam sample with a different shape to the

55 mould [19,23,40]. Applying different compression regimes to different foam regions during
56 fabrication can produce gradient open cell auxetic foams. Stretching foams in one or more
57 directions by passing pins through the foam during fabrication produces long, re-entrant cells,
58 increasing Young's modulus and the magnitude of positive or negative Poisson's ratio during
59 loading parallel to the long cell axis [38,40,41]. Foam in personal protective equipment is often
60 segmented so it fits the body better than a continuous sheet [42–44], but any reduction or loss
61 of padding between segments may reduce protection. Varying material properties in running
62 shoe midsole regions can influence and improve running style [45]. Gradient foams may offer
63 benefits to personal protective equipment and footwear in terms of how they comfortably
64 cover, deform with and protect body segments [19,23,40].

65 Chan and Evans found thermo-mechanical fabrications to rupture closed cell foam
66 walls during fabrication [21,46]. Fabrication methods for auxetic closed cell foams that do not
67 rupture cells use hydrostatic compressive pressure applied by a pressure vessel [47], or steam
68 absorption and condensation [48,49]. Cell structure, Poisson's ratio and Young's moduli of
69 closed cell auxetic foams vary with compression imparted following fabrication, with common
70 volumetric compression ratios (original/final volume) being between 1.3 and 6.0 [47–49]. Of
71 the two available options for fabricating closed cell auxetic foam, the steam fabrication method
72 uses simpler equipment, such as a steam bath or an oven and a water filled container [48,49].
73 Upon cooling, as the foam shrinks and cell walls become re-entrant, the constituent polymer in
74 some foams, such as polyethylene, passes through a thermal transition that fixes the imposed
75 cell structure [48,49]. Absorbed water can, then, evaporate from the foam within a week of
76 fabrication, leaving a stable auxetic closed cell foam with negligible trapped water [48,49].

77 Auxetic and conventional closed cell foam characteristics have been explained using
78 dimensions estimated from two-dimensional (2D) projections of cell structures, based on
79 microscopic imaging. Analytical models for conventional and auxetic foam consider the

stretching, flexing and hinging of cell ribs to predict Poisson's ratios and Young's moduli [40,41,50]. No analytical model has been published considering infrequently researched auxetic closed cell foams. Analytical models for conventional closed cell foams have combined the effects of gas pressure on cell rib and wall deformation, estimating dimensions and orientations from 2D cell projections [41,51,52].

Auxetic closed cell foam fabrications that rely solely on pressure differentials offer limited control over compression [47–49]. As such, before beginning a study fabricating a new type, size or shape of auxetic closed cell foam, pilot work is needed to find the processing conditions that give the desired volumetric compression. Gradient or intentionally anisotropic auxetic closed cell foams have not previously been produced. This work explores two steam fabrication-based methods to control cell structure modification in different axis and foam regions. These fabrication methods were: i) Constraining or stretching foam regions, using pins, to produce intentionally anisotropic gradient foam, and ii) Preventing steam from reaching regions of a sample, to produce gradient foam. The effect of these methods and modifications to cell structure, on Young's modulus and Poisson's ratio, are explained by combining analytical models for open cell auxetic foam [40] and the effect of gas pressure in closed cell foam [51,52].

2. Methods

2.1. Fabrication

Two sheets ($210 \times 110 \times 10$ mm) and two cuboids ($200 \times 20 \times 10$ mm) of closed cell foam (Plastazote LD-60, algeos.com), pre-conditioned for a week in an environmental chamber (20°C and 10% relative humidity), were fabricated by steam processing [48,49]. One sheet of foam was unconstrained during fabrication. The other sheet was constrained at one end by twelve steel pins ($\varnothing 2$ mm) passed through holes in aluminium plates ($100 \times 100 \times 2$ mm), sandwiching but not compressing the foam (Figure 1a). Pins were inserted in each corner and

1
2
3 105 along each side of the plates with 33 mm spacing. The central 45 mm of one cuboid (i) was
4
5 106 stretched to 1.5 times its original length, using four pins passed through the foam and an
6
7 107 aluminium box section (surrounding but not touching) to hold the pins apart (2 mm thick walls,
8
9 108 $22 \times 22 \times 65$ mm Figure 1b). Foam samples and constraining devices were placed in 250×350
10
11 $\times 40$ mm aluminium dishes (2 mm thick walls) filled to ~ 30 mm with water and covered with
12
13 109 aluminium foil [49]. Cuboid (ii) was positioned with half its length inside an aluminium drinks
14
15 110 can ($\varnothing 70$ mm, height 100 mm, 1 mm wall thickness), filled to 80% with water, and with a ~ 15
16
17 111 $\times 15$ mm hole in the top. The foam was passed through the hole in the can, so the upper half
18
19 112 was dry heated during fabrication (Figure 1c).
20
21 113

22
23
24 114 All containers were heated in an oven (MCP Tooling Technologies LC/CD, $\pm 0.25^\circ\text{C}$) set
25
26 115 to 105°C for 4.5 hours [49]. After steaming, samples and constraining devices were removed
27
28 116 from the containers and cooled for 30 minutes on a drying rack in an air-conditioned laboratory
29
30 117 with an expected temperature of 20 to 25°C and relative humidity of 30 to 60%. Samples began
31
32 118 to shrink upon removal from the water, with shrinking appearing to finish within 1 to 2 minutes.
33
34 119 Constraining devices were then removed, and samples were returned to the environmental
35
36 120 chamber for a week before testing. The order of cutting (Figure 1d), and testing, is shown in
37
38 121 Figure 1e (tensile tests, then compression tests or micro-ct). Samples were returned to the
39
40 122 environmental chamber between tests. Tests were in the air-conditioned laboratory described
41
42 123 above (20 to 25°C and relative humidity of 30 to 60%).
43
44
45
46
47
48
49
50
51
52
53
54
55
56
57
58
59
60

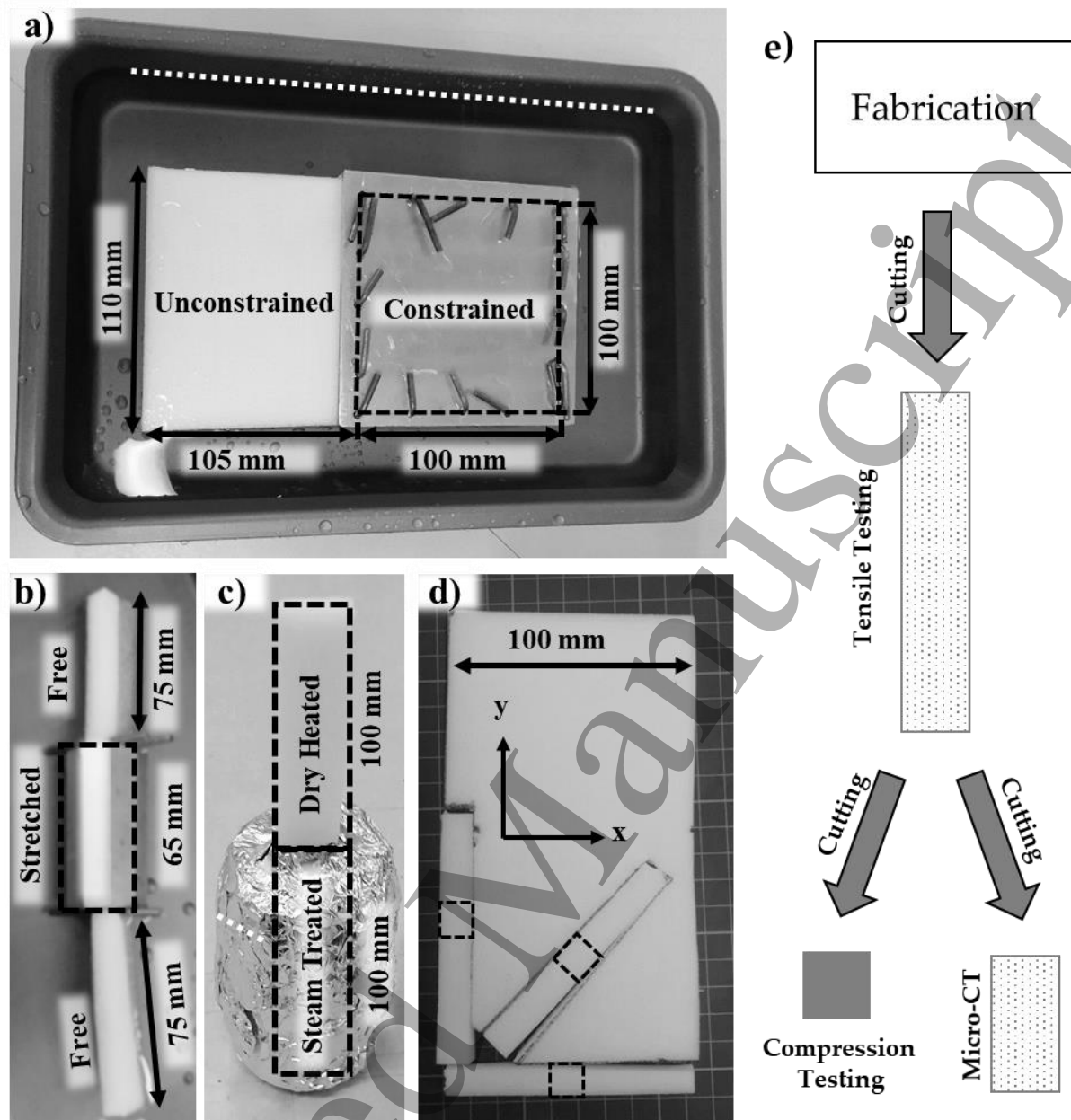


Figure 1. a) Sample containing constrained region (note the 5 mm edge surrounding the constrained region); b) Sample containing stretched region; c) Sample half steamed and half dry heated; d) Example tensile cuboids and compression (dashed lines) with sample orientations, locations and axis labelling marked; e) Order of sample preparation. The same orientations and co-ordinate systems were used for all sheets/regions. Y-axis parallel to sample length, x to width in (b) and (c). White dotted lines in (a) and (c) show water level.

2.2. Characterisation

Mass (Sartorius, M-power) and dimensions (Vernier Calipers) of all samples and regions were measured before and one week after fabrication, to see if any cells contained water, which would increase mass, and to measure linear compression ratios in each orthogonal axis (LCR, final/original length). The partially open cells on the faces of foam samples do not

shrink during fabrication as they cannot trap steam [48,49]. Therefore, 1 to 2 mm was cut from the planar edges of converted samples with a utility knife (Stanley) before characterisation. The top and bottom faces were not removed, as samples were already thin (3 to 5 mm). Three samples of unconverted foam ($100 \times 10 \times 10$ mm), foam from the unconstrained sheet and from each region of the gradient sheet ($\sim 60 \times 5 \times 5$ mm) were cut for tensile tests, with the utility knife, at 45° increments (Figure 1d). The two cuboids were cut for tensile testing, with one $\sim 60 \times 5 \times 5$ mm sample taken from each region (three samples in Figures 1b and two in c). The dimensions and mass of the tensile samples were used to calculate final density ratio (FDR, final/original density).

A speckle pattern was applied to all samples (matt Acrylic spray paint, Halfords) for full-field strain measurement using 2D digital image correlation (DIC). Tensile tests were at a strain rate of 0.0033 s^{-1} to 10% tension on an Instron 3369 with a 500 N load cell sampling at 25 Hz. Samples were clamped ~ 10 mm from their ends in the jaws of the device, which were closed to 1 mm, giving gauge lengths of 40 to 80 mm. These cuboidal samples had longer gauge lengths (>35 mm) and were thinner than the 12 mm sided 'dog-bone' samples specified in ASTM D3574 – 11, to account for end effects [53]. Tensile tests were filmed with a camera (**Figure 2a**), with its image plane aligned to a face of the sample (LaVision DIC package, 1260×1080 p, 10 fps, Nikon lenses with 100 mm optical zoom). A target area was defined over the central lengthwise third of samples (Figure 2b & c), giving axial and transverse true strains, with facet sizes set to give at least three speckles per facet (10 to 15 pixels) [54]. Device jaws were rotated 90° around the loading axis between tests, with the sample in place, to apply strain mapping to four faces. Sample cross sectional areas were measured before each test with Vernier Calipers to allow stress to be calculated.

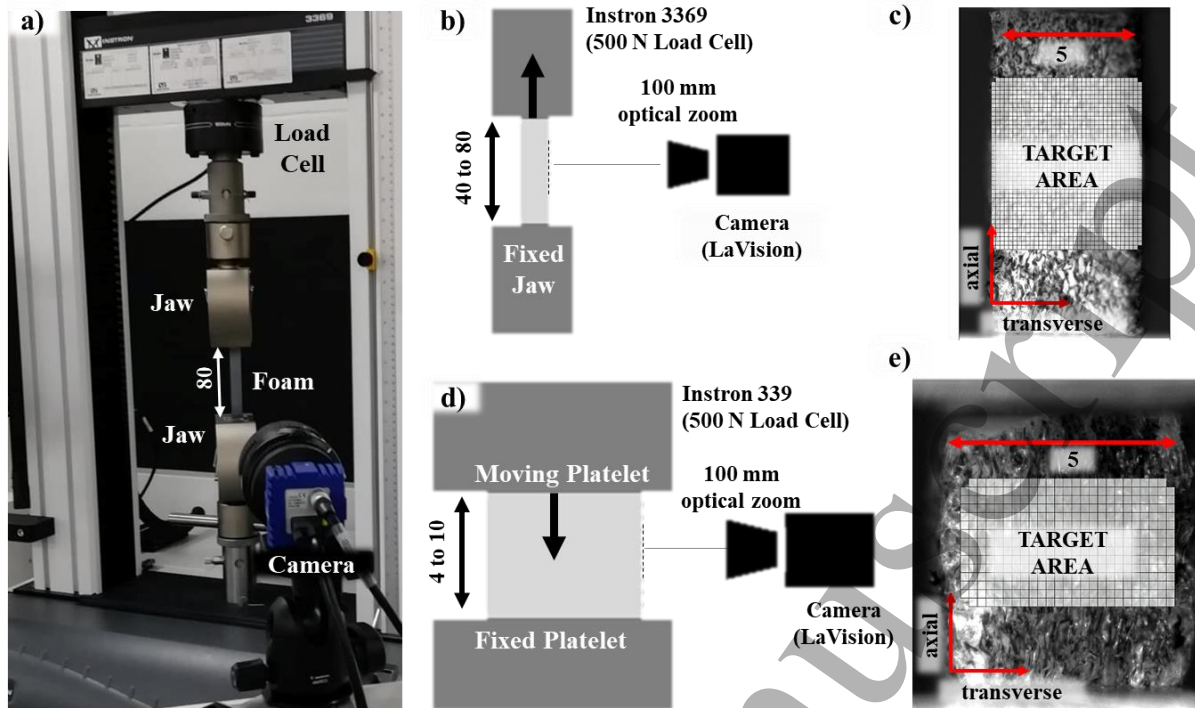


Figure 2. a) Tensile sample and camera, b) Tensile test schematic; c) tensile sample with speckle pattern and target area; d) compression test schematic; e) compression tests sample with speckle pattern and target area. Dimensions in mm.

Cubes for compression testing (4 to 10 mm sided) were cut from the lengthwise centre of all tensile samples one day after testing, and dimensions were measured (Figure 1d). These cubes were smaller than specified in ASTM D3574 – 11 due to the low initial foam thickness [53]. Three cubes were cut from the stretched region of the gradient cuboid in Figure 1b to allow repeat testing of the only foam that was stretched during fabrication. Cubes were compression tested in all three orthogonal axes between platelets using the same equipment and settings as the tensile tests (Figure 2d & e) and a preload of 0.1 N to ensure contact, corresponding to 0.25 to 0.75% compression. Incremental Poisson's ratios were calculated by fitting linear trend lines to transverse vs. axial engineering strain data (from DIC, same system as tensile tests) at 0.5 or 1% axial strain increments, depending on the number of available data points for regression fitting. Incremental tangent moduli were calculated in the same way, from stress vs. axial engineering strain data from Instron's software Bluehill 4.0's force and

displacement, and measured sample dimensions. Young's moduli were taken as the tangent moduli at the lowest calculated axial strain (up to 0.5 or 1%).

To see cell shapes, micro-computed tomographic (micro-ct) scans of $\sim 5 \times 5 \times 20$ mm samples from each region of each type of foam were collected (SkyScan 1172; 360° rotation, image acquisition every 1.4°, resolution < 5 μ m). Micro-ct data were rendered (SkyScan, CTVox) and images taken of one cell (~ 100 to 500 μ m) deep volumes in each orthogonal axis. To help compare cell structures, single cell images were processed by removing unconnected pixels with areas under 2% of the cell using erosion functions (*imclose* and *bwareaeopen*) in MATLAB® 2019a (Mathworks, USA).

2.3. Analytical Modelling

Analytical models based on 2D cell projections [40], and the effect of air pressure based on analysis of the same polyethylene foam of lower density (LD-24, Zotefoam) [51], were combined and adapted. The adapted model was used to explain Young's moduli (E_y and E_z) and Poisson's ratios (ν_{yz} and ν_{zy}) at 0.75% compression and tension (ϵ_y and ϵ_z). The value of $\pm 0.75\%$ strain was selected as the 2nd data point in most Tangent moduli and Poisson's ratio vs. strain data. Details of the model for 2D cell projections, taken from previous open cell foam work [40], are included as Supplementary Material S2, with unitless dimensions relative to the vertical rib length ($h = 1$, which is diagonal rib length). Some changes to cell dimensions were made from the previous study [40]. As low cell wall thickness is common in closed cell foams [41,51], relative rib/wall thickness was halved from 0.2, as used in the previous open cell foam work [40], to 0.1 (Figure S6). Cell walls were partially constrained by gas pressure; increasing the relative amount of stretching, rather than flexure and hinging, as discussed elsewhere [51]. With the support from the internal air pressure, rather than reducing the flexure and hinging constant (k_{hf}) for the thinner walls, k_{hf} was increased from 0.04 [40] to 0.10 in tension. Cell walls of unconverted closed cell foam begin to buckle at low (0 to 3%) compression [51]. Since

many of the converted foams had kinked cell walls from fabrication, buckling was expected to occur at close to 0% compression, so k_{hf} was reduced three-fold (to 0.03) in compression, which was an arbitrary amount found to fit the data. Sensitivity to variations in k_{hf} are shown in the supplementary material (Figure S5). The force constants for flexing and hinging were unchanged from the previous model (0.04 and 0.0044, respectively) [40]. To account for gas pressure, relative volumetric deformation (Equation 1) was [51,52]:

$$\varepsilon_v = \frac{\varepsilon_u}{(1 - \varepsilon_u - R)} \quad (1)$$

where relative density (R) was the density of polyethylene (~900 kg/m³ [51]) divided by the measured foam density, and ε_v and ε_u were volumetric and uniaxial strains, respectively. The contribution of air pressure (p_{air}) to Young's modulus (E_{air} , Equation 2) was [51]:

$$E_{air} = \frac{p_{air}}{\varepsilon_u} = \frac{\varepsilon_v * p_0 * (1 - 2\nu)}{\varepsilon_u} \quad (2)$$

where p_0 was air pressure inside cells before testing, which was assumed to be atmospheric pressure (100 kPa) [51]. The foam modulus ($E_{combined}$) was calculated by adding the gas pressure contribution from Equation (2) and cellular modulus (E_{cell}) from Equation (S5) [51].

$$E_{combined} = E_{PE} * E_{cell} + E_{air} \quad (3)$$

where E_{PE} was the Young's modulus of polyethylene (300 MPa) [51]. Values for E_y and E_z were normalised to E_y from the analytical model at 0% strain and multiplied by the mean of measured compressive and tensile E_y . The combined Poisson's ratio ($\nu_{combined}$) was:

$$\nu_{combined} = \nu_{cell} + \nu_{fluid} * \frac{E_{air}}{E_{trans-cell}} \quad (4)$$

where ν_{cell} was the cellular Poisson's ratio contribution (ν_{cell} , Equation S6), ν_{fluid} was the Poisson's ratio of a fluid (of 0.5) and $E_{trans-cell}$ was the cellular transverse Young's modulus. Estimating the effect of trapped gas on Young's modulus and Poisson's ratio, rather than calculating its effect on cell rib deflection, means this analytical model can only show trends at low strains (< 1%).

1
2
3
4
5
6
7
8
9
10
11
12
13
14
15
16
17
18
19
20
21
22
23
24
25
26
27
28
29
30
31
32
33
34
35
36
37
38
39
40
41
42
43
44
45
46
47
48
49
50
51
52
53
54
55
56
57
58
59
60

3. Results

3.1 Sample measurements

Foam density increased (from $50.2 \pm 0.8 \text{ kg/m}^3$, mean \pm standard deviation (S.D.)) for the steamed samples following fabrication, giving FDRs between ~ 3 and 4 (**Figure 3a**). Density was unchanged (FDR = 1.0) for the dry heated region of foam that was not exposed to steam (in Figure 1c). Change in mass after a week in ambient conditions, before any other testing, was negligible (up to 0.3%), indicating any trapped water had evaporated and any increase in sample density was likely due to a decrease in volume. Unconstrained regions (FDR between 3.5 and 4.0) shrank more after fabrication than constrained regions (FDR between 3.0 and 3.5).

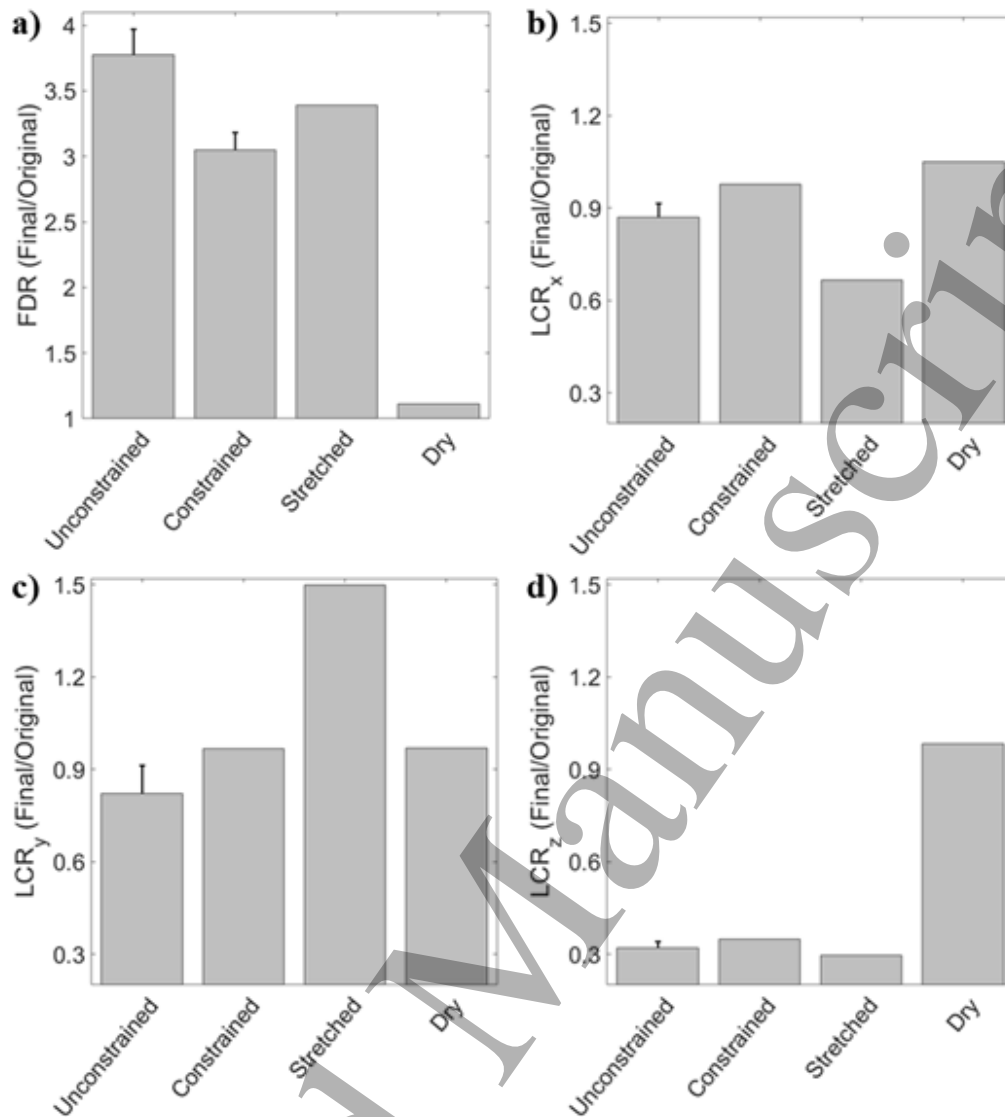


Figure 3. a) Final density ratio of samples cut for tensile testing and; b) to d) linear compression ratios measured from whole processed samples, parallel to the b) x-axis (shorter side), c) y-axis (longer side), and d) z-axis (through thickness). Same legend (d) for all. Error bars show 1 S.D. for conditions where multiple samples were fabricated.

Considering the unconstrained, steamed foam samples and regions, planar (x and y) LCRs (Figure 3b & c) were about 0.9, with more through thickness shrinking ($LCR_z \approx 0.3$, Figure 3d). The constrained region of the gradient sheet exhibited planar LCRs of 1.0 (i.e. unchanged, due to the constraints) and an LCR of 0.3 through thickness. The stretched region of the steamed cuboid retained its applied LCR of ~ 1.5 in its y-axis (Figure 3c), an LCR of 0.7 in the x-axis (Figure 3b) and similar through thickness LCR to other samples ($LCR_z \approx 0.3$, Figure 3d).

3.2 Cell Structures

There was negligible difference in cell structure between orientations for the unconverted foam (Figure 4a to c), suggesting little to no elongated cell rise [41], as expected [49]. Steam contraction in the unconstrained sheet (Figure 4d & e) reduced cell size and imparted different topology, corresponding to some kinks in the previously straight cell walls, which were most obvious through thickness (Figure 4d). The structure of cells on the outer faces of samples barely changed following fabrication, as cells on the outer faces were partially open from cutting and could not trap steam (Figure 4f). Constraining foam in two directions created a similar effect to the unconstrained conversion, except the cells were wide, with low thickness (Figure 4g), but similar to the unconverted foam (Figure 4a to c) in the constrained x-y plane (Figure 4h) and on their outer faces (Figure 4i). Stretching foam in the y-axis also produced a similar effect, with wider, thinner cells still (Figure 4g), and different topology, corresponding to some kinked cell walls in the x-y plane (Figure 4k), caused by contraction in the x-axis ($LCR_x = 0.7$, Figure 3b). The outer faces of steamed samples had hexagonal cells, which were longer in their stretched y-axis for samples stretched by pins during fabrication (Figure 4l).

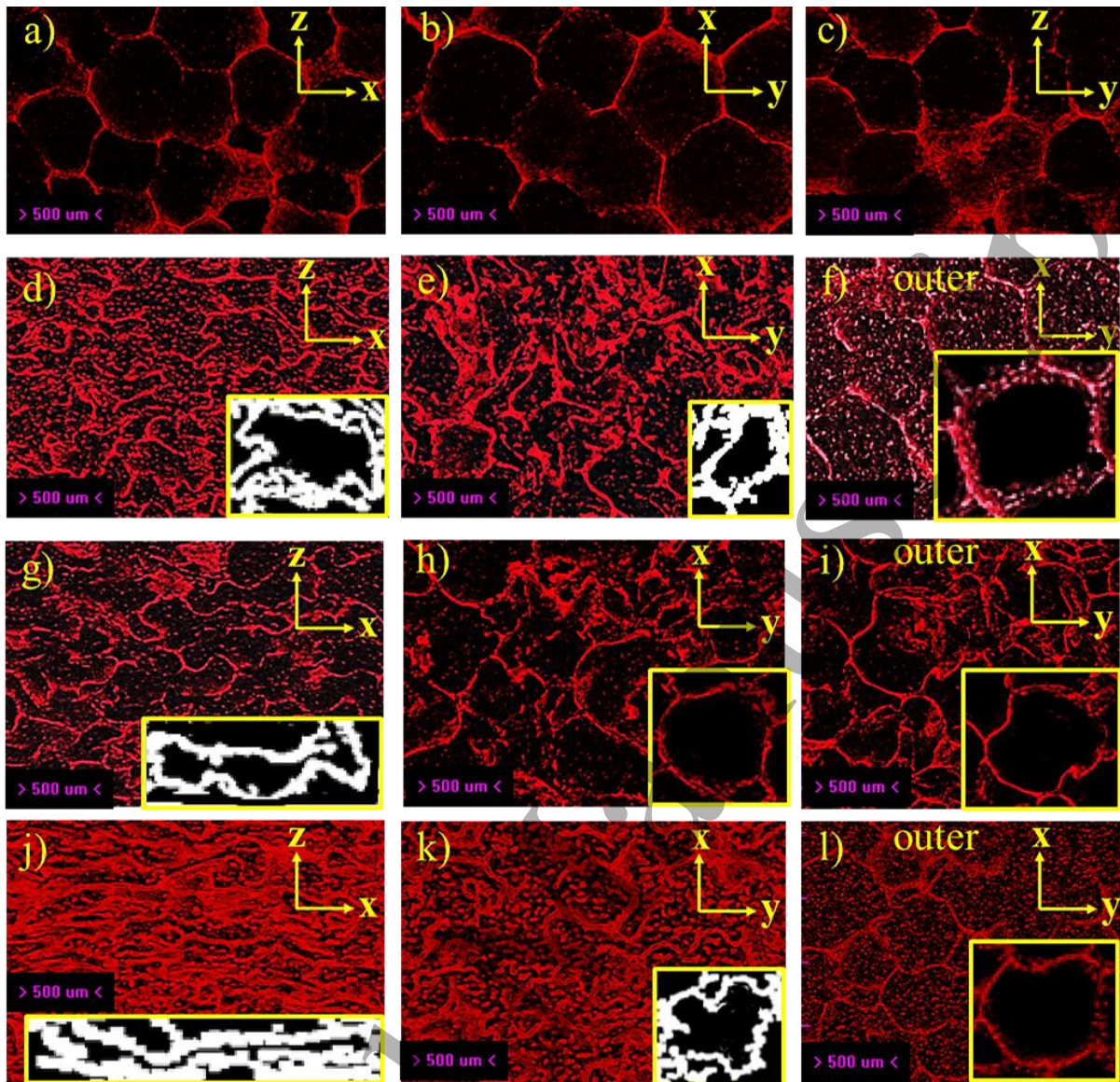
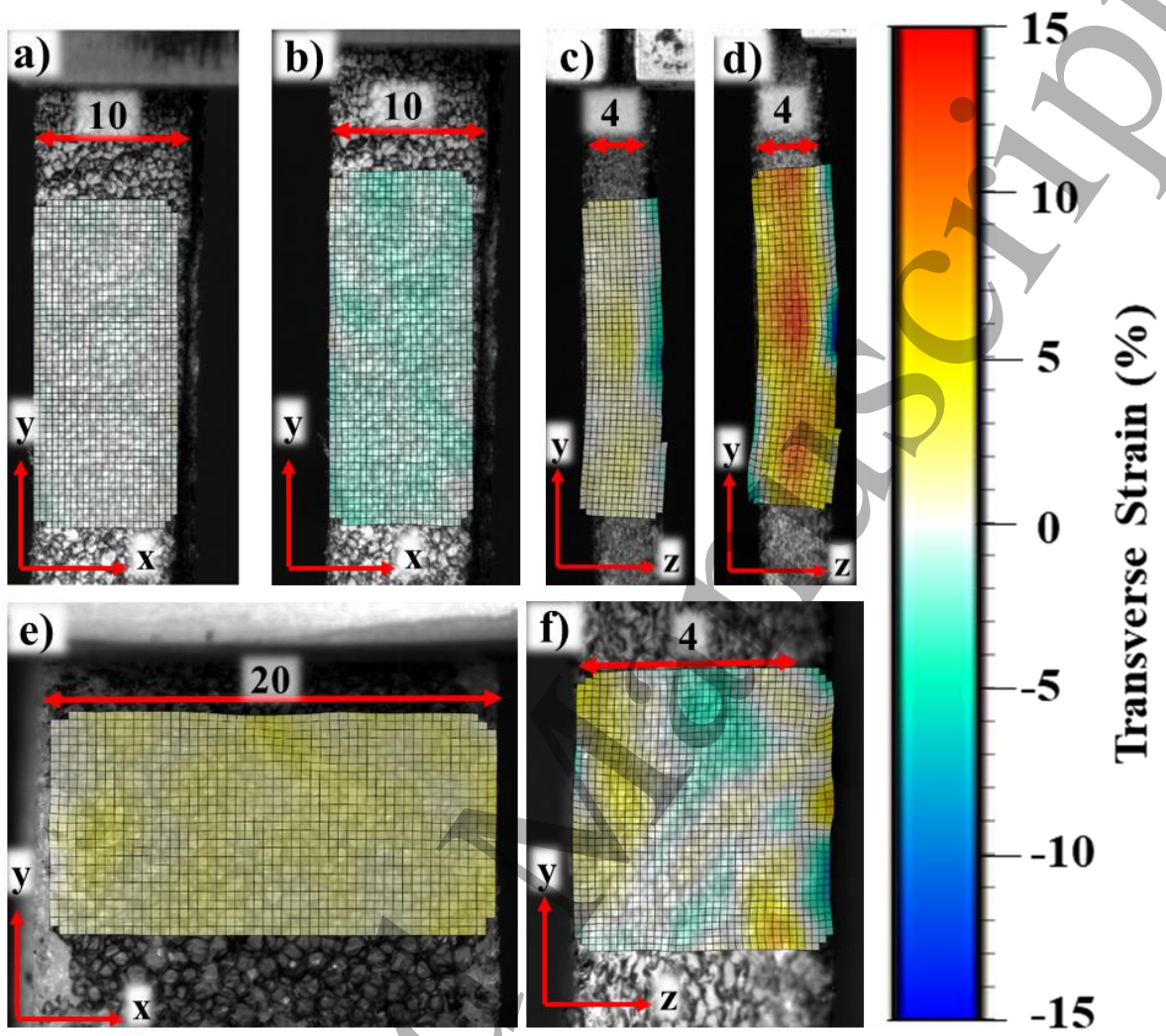


Figure 4. Micro-ct scans of a) to c) unconverted foam; d) to f) unconstrained, steamed sheet sample, g) to i) the constrained region of the constrained sheet, j) to l) the stretched region of the partially stretched gradient cuboid. Labels show orientation, subfigures f, i) and l) show steamed foam's outer face. Inserts in d) to l) show processed single cell images digitally expanded by 1.5 times their original size. White single cell images were processed in MATLAB®, others by minor manual editing to accentuate cell walls.

3.3 Digital Image Correlation

Contour plots of transverse strain from DIC show the unconverted foam contracted transversely at 2 and 10% tension (**Figure 5a & b**) and the auxetic foam expanded (Figure 5c & d). Contour plots at 10% compression show the unconverted foam expanded transversely (Figure 5e). The auxetic sample contracted transversely at the centre (Figure 5f) and expanded along the edges; corresponding to regions with (Figure 4g) and without (Figure 4i) re-entrant

1
2
3
273 cell structures, respectively. See supplementary video for strain mapping of uniform and
4
5
274 gradient samples in tension.
6
7
8
9



275
276 **Figure 5.** Contour plots of transverse strain from DIC of a) and b) unconverted foam at a) 2% and b) 10% tension;
277 c) and d) the constrained region of the gradient sheet at c) 2% and d) 10% tension; e) unconverted foam at 10%
278 compression; f) the constrained region of the gradient sheet at 10% compression. Labelled dimensions are in mm.

279 **3.4 Stress and lateral strain vs. axial strain**

280 NPR behavior (i.e. contraction) of the unconstrained foam was retained to ~2 to 3%
281 compression (**Figure 6a**), followed by transverse expansion. The constrained region of the
282 gradient sheet had a steeper compressive axial vs. transverse strain relationship and therefore
283 a higher magnitude of (negative) Poisson's ratio than the unconstrained region. NPR was,
284 however, only maintained to ~1% compression in the constrained region. Tensile transverse
285 vs. axial strain was quasi-linear for all samples (Figure 6b), with the constrained region of the
60

gradient sheet expanding more transversely than the unconstrained region. The unconverted foam exhibited transverse expansion in compression (Figure 6a) and transverse contraction (Figure 6b) in tension.

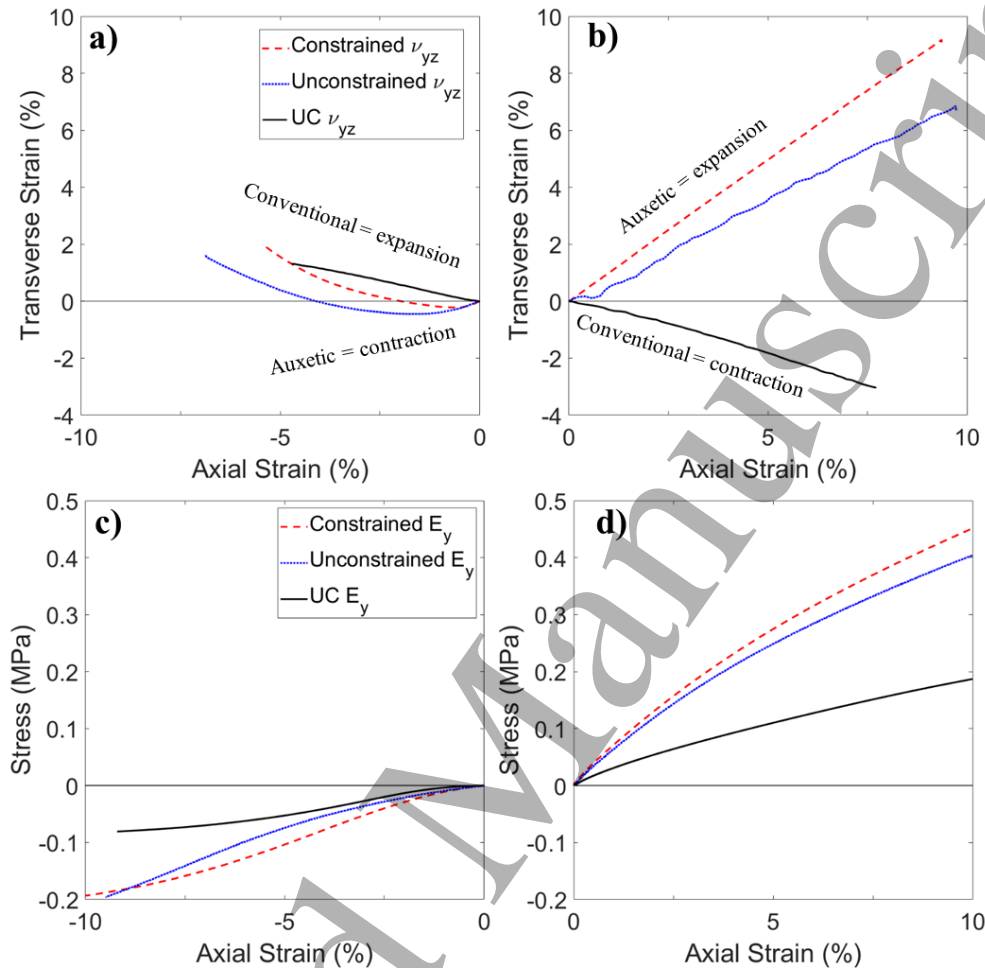


Figure 6. Sample plots of a) & b) Transverse vs. axial strain in a) compression and b) tension; c) & d) Stress vs. axial strain for constrained and unconstrained regions of the gradient sheet, and the unconverted foam in c) compression and d) tension. Negative strain values indicate axial compression and transverse contraction. Same legend applies to a) & b), and c) & d).

The unconverted foam exhibited its characteristic stress vs. strain plateau at ~5% compression [41,49,55] (Figure 6c). The constrained region of the gradient sheet also had a stress vs. strain plateau, at ~8% compression, and a steeper initial gradient and therefore higher Young's modulus than both the unconverted and unconstrained regions. The unconstrained region exhibited linear stress vs. strain of steeper gradient than the unconverted foam. In tension (Figure 6d), stress vs. strain relationships of all samples were quasi-linear, with the

1
2
3
4
5
6
7
8
9
10
11
12
13
14
15
16
17
18
19
20
21
22
23
24
25
26
27
28
29
30
31
32
33
34
35
36
37
38
39
40
41
42
43
44
45
46
47
48
49
50
51
52
53
54
55
56
57
58
59
60

same order of low to high Young's moduli as in compression (unconverted < unconstrained < constrained).

3.5 Poisson's ratios

The unconverted sample was isotropic ($\nu \approx 0.4$, **Figure 7a & b**, Supplementary Material S1). Measured Poisson's ratios and tangent moduli of test samples cut from unconstrained regions of different fabricated samples were similar to each other (Figures S1 & S2). A selection of samples, from the constrained and stretched regions of gradient foams, demonstrating the different mechanical behaviors and imparted cell structures are outlined here. Detailed results are included in the supplementary material (Figures S1 & S2), along with collated Young's modulus and Poisson's ratio data (Supplementary Table S1). The mechanical properties of the dry heated region of foam were similar to the unconverted foam (Figures S1 & S2), as FDR and LCRs were ≈ 1 , so cell structures were unchanged (Figure 3).

Concerning the gradient sheet, tensile and low strain (<0.5%) compressive Poisson's ratios of the unconstrained section were as low as -0.7 (ν_{yz} , Figure 7a & b). In the slightly compressed in-plane directions (LCR ≈ 0.9), Poisson's ratios ($\nu_{xy} \approx 0.1$) were lower than for the unconverted foam. During through thickness compression tests, ν_{zy} was about zero. In the unconstrained foam section (Figure 7c & d), Poisson's ratio had greater anisotropy; NPR reached a higher magnitude ($\nu_{yz} \approx -1.0$), whereas the in-plane Poisson's ratio was closer to that of the unconverted foam ($\nu_{xy} \approx 0.2$). Through thickness compressive Poisson's ratio (ν_{zy}) was also close to zero (Figure 7c). Trends in the stretched region (Figure 7e & f) were broadly similar to the constrained region, but the positive Poisson's ratio ν_{yz} (of 1) was higher in compression; as in similar work stretching open cell foam during fabrication [38,40].

Calculated Poisson's ratios, based on Equation (4) and schematics in Supplementary Figure S3, show reasonable agreement (within ~ 1 S.D.) with measured values (Figure 7 & Supplementary Material S2). The analytical model predicts that the effect of transverse

expansion of gas in compression increases with cell anisotropy (Supplementary materials Figure S4 -S8), as does Figure 7 data. NPR (ν_{yz}) was present up to 2 to 3% compression for the unconstrained region (Figure 7a) and 1 to 2% for the constrained region (Figure 7c), whereas the stretched foam had positive compressive Poisson's ratio (Figure 7e).

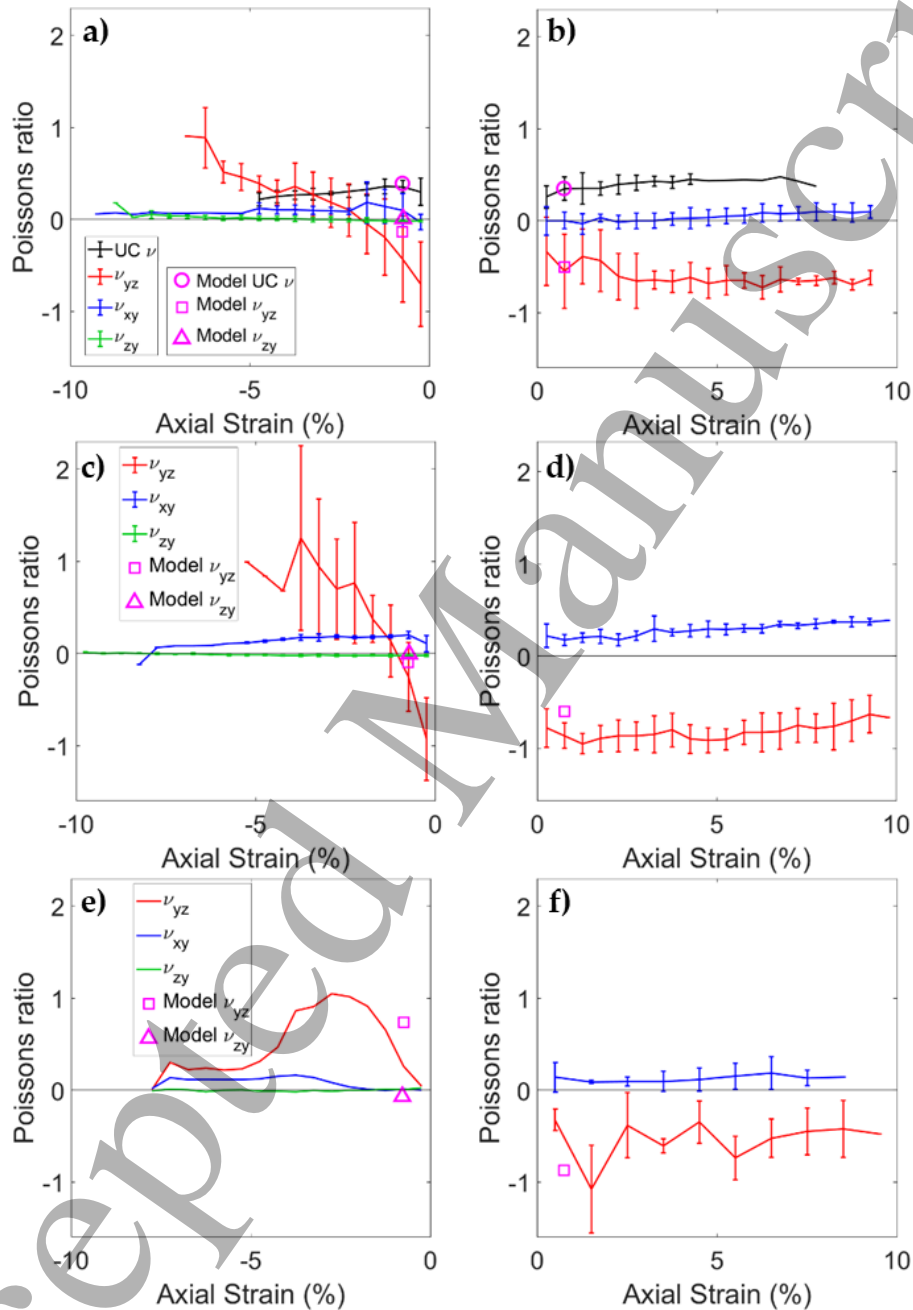


Figure 7. Measured and calculated (Equation 4) Poisson's ratio vs. axial strain for; a) & b) unconverted and unconstrained foam (samples from the gradient sheet, a) in compression, b) in tension), c) & d) constrained foam from the gradient sheet (c) in compression, d) in tension), e) & f) the stretched section of the gradient cuboid sample (e) in compression, f) in tension). Data for axial and transverse strain parallel to the x and y-axis or at 45° were combined. Mean values and error bars showing 1 S.D. are plotted, except for in (e) where median values were plotted in compression. Legends in a), c) & e) apply to b), d) & f), respectively. All samples and orientations are included in Supplementary material S1 and data is also included in Table S1.

1
2
3
4
5
6
7
8
9
10
11
12
13
14
15
16
17
18
19
20
21
22
23
24
25
26
27
28
29
30
31
32
33
34
35
36
37
38
39
40
41
42
43
44
45
46
47
48
49
50
51
52
53
54
55
56
57
58
59
60

3.6 Tangent moduli

Unconverted foam exhibited tangent moduli of ~1 MPa up to ~5% compression (**Figure 8a**), with a reduction to ~0.5 MPa when it entered the plateau region (Figure 6c), and of ~2.5 MPa up to 10% tension (Figure 8b). In compression, both regions of the gradient sheet (Figures 8a & c) were stiffer through thickness ($E_y \approx 2.5$ MPa at 5% compression) than in plane (E_x & $E_y \approx 1$ to 1.5 MPa). Planar tensile Young's moduli were lower in the unconstrained region (E_x & $E_y \approx 7$ MPa, Figure 8b) than the constrained region (E_x & $E_y \approx 8$ MPa, Figure 8d). Compressive tangent moduli parallel to the x and y-axis tended to be higher in the constrained region (~1 to 2 MPa, Figure 8c) than the unconstrained region (~0.5 to 1.5 MPa, Figure 8a), but lower (both ~1 to 2 MPa) when loaded parallel to the z-axis. When loaded along the stretched (y) axis, the stretched region of the gradient cuboid was stiffer (Figure 8e & f) than other orientations and samples; both in compression (tangent modulus up to 4 MPa, Figure 8e) and tension ($E_y \approx 12$ MPa, Figure 8f), agreeing with trends in previous work stretching open cell foam during fabrication [40,56]. Young's moduli are also in Supplementary Table S1.

Differences in both tensile and compressive tangent moduli between regions agree with increased anisotropy in Poisson's ratio measurements (Figure 7), micro-ct images of cell structures (Figure 4), LCRs (Figure 3) and the analytical model (Figure 8). Equation 3 also predicts Young's moduli to within ~1 S.D. of the mean measured value (Figure 8). As with Poisson's ratio measurement and calculations, the lower stiffness in tension supports increased cell wall flexure and bending in compression.

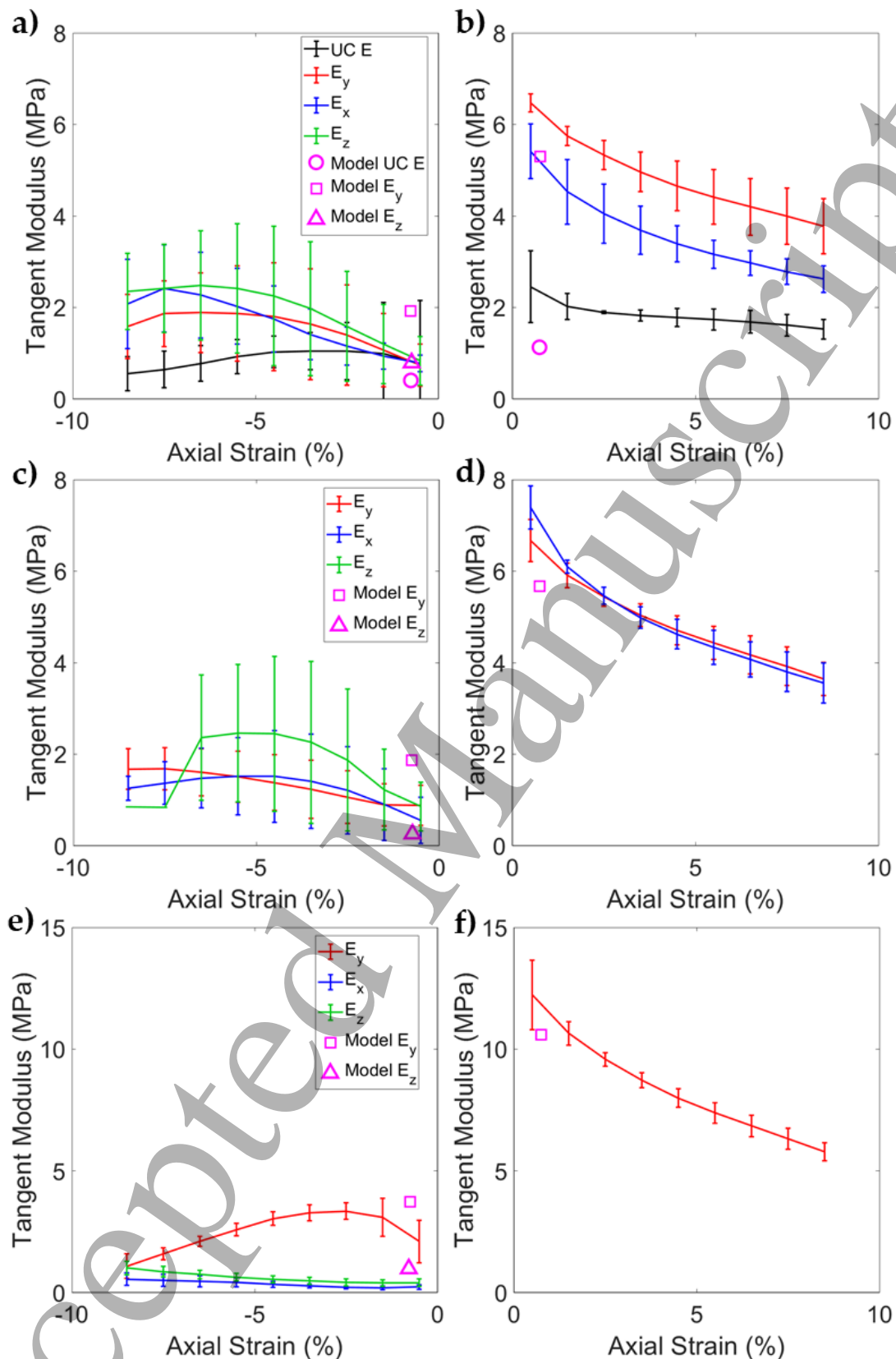


Figure 8. Mean and calculated (Equation 3) tangent moduli of a) & b) unconstrained and unconverted foam (samples from the gradient sheet) in a) compression and b) tension; c) & d) the constrained section of the gradient sheet in c) compression and d) tension; e) & f) the stretched section of the gradient cuboid in e) compression and f) tension. Error bars show 1 S.D. All samples and fabrication shown in Supplementary material S1, and data is replicated in Table S1.

4. Discussion

Constraining, stretching or preventing steam from reaching regions of closed cell foam allowed control over cell structure during steam conversions (Figure 3). Constraining and stretching foam regions during fabrication increased anisotropy in gradient foam regions. Comparison with an analytical model, adapted from previous works [40,51], showed agreement (within ~ 1 S.D.) between imparted LCRs (Figure 3) and cell structures (Figure 4), with measured Poisson's ratios (Figure 7) and Young's moduli (Figure 8). The imparted cell structures of regions of auxetic foam that were unconstrained during fabrication look similar to those in previous work, and agree with an analytical model [48,49]. Further work could steam larger and thicker samples of constrained foam, to allow for compression tests that comply with ASTM D3574 – 11 [53].

Regions of foam unconstrained during fabrication, from different samples, exhibited similar mechanical properties, including Poisson's ratios (lowest $\nu_{yz} \approx -0.7$, Figure 7, Figure S1) and tensile Young's moduli of ~ 7 MPa (Figure 8b, Figure S2). The gradient sheet had a slight gradient along its y-axis (e.g. $\nu_{yz} \approx -0.7$ to -0.8 , tensile $E_y \approx 7$ to 8 MPa), as expected and predicted by the analytical model (Figures 7c, 7d, 8 c, 8d). The two cuboids had clear gradients between regions: i) Unconstrained regions were similar (e.g. $\nu_{yz} \approx -0.7$, tensile $E_y \approx 7$ MPa); ii) The stretched region had similar tensile ν_{yz} of ~ -0.5 (Figures 7c) but higher tensile E_y of ≈ 12 MPa (Figure 8f); iii) The dry-heated region was similar to the unconverted foam (Figures 7a, 7b, 8a, 8b), with $\nu \approx 0.4$ and $E \approx 2.5$ MPa (Figures S1f and S2f).

The effects of modifying cell structure agreed with our understanding of open and closed cell foam, including: i) analytical models of auxetic and conventional open cell foam [40,41,50]; ii) analytical models of conventional closed cell foam [41,51,52], and; iii) previous tests of auxetic closed cell foam [47–49]. Cell structure (Figure 4h) and Poisson's ratio (Figure 7a & b) in directions constrained (LCRs = 1), but not stretched, by pins during steaming were similar to that of the unconverted foam. Young's moduli of the converted foam did, however,

tend to increase with foam density from shrinkage in the unconstrained through thickness direction (Figures 3a, 8a & 8b). Kinked cell walls and smaller cells imparted by the steam process (Figure 4e & f) gave NPR (Figure 7a & b) and increased Young's modulus (Figure 8a & b), as in previous work with open cell foam [19,23,38,40].

Considering the gradient sheet, constraining the foam (and cells) during fabrication, and volumetric shrinking during cooling - when the polyethylene was softened by the remaining heat - is likely to have increased the diagonal rib length (i.e. l in Figure S3). Increasing the relative diagonal cell wall length in the analytical model increased transverse strain ($\epsilon_{\text{transverse}} \propto l/h$, whereby h is vertical rib length, Supplementary Figure S3) and the magnitude of cellular NPR (ν_{yz} , Figure S7a), agreeing with mechanical test data and clearest in tension (e.g. Figure 7a to d). The increased magnitude of NPR would, then, be expected to increase volumetric deformation, and therefore changes in internal air pressure, increasing stiffness ($E_{\text{combined}} \propto E_{\text{air}} \propto \epsilon_v$, Equation 2), as in Figure 8a to d [51].

Compressive and tensile characteristics of the steamed foams differed, depending on the specifics of fabrication. NPR was maintained to higher tension (10%) than compression (~2%, Figure 7), suggesting more implications for fit of personal protective equipment, and prosthetics, than indentation or impact performance, although this was not tested specifically. Previous work suggested that cell wall buckling began at low (0 to 3%) compression of closed cell foams [51]. The analytical model (Equations 3 & 4) predicts negative tensile Poisson's ratio (ν_{yz}), but near zero or positive compressive Poisson's ratio (ν_{yz} , Figure 7), and reduced compressive stiffness (E_y , Figure 8), as cell walls buckle. Lengthening cells, by stretching foam in the y-axis during fabrication (Figure 4j), increased stiffness in the y-axis (E_y , Figure 8e & f) [23,57], and gave positive compressive Poisson's ratio (Figure 7e).

Before considering internal air pressure, the analytical model and previous work in open cell foam [40], suggest compressive NPR, and low compressive transverse stiffness, as cell

414 wall flexure and bending increase (Figure S5, [40]). With their low transverse stiffness, air
 415 trapped in the cells caused transverse expansion and positive compressive Poisson's ratio
 416 (Figure 7 and Equation 4). The effect of air pressure in the closed cells, and the compression
 417 level at which positive Poisson's ratio occurred (Figure 7a, c & e), increased with the diagonal
 418 cell wall length (Supplementary Figure S3 b to d), as relative transverse stiffness decreased
 419 (Figure 8) [40]. Further work could develop this auxetic closed cell foam analytical model for
 420 larger strains.

421 Unlike most auxetic open cell foams, the closed cell auxetic foams reported here had
 422 similar compressive stiffness (~1 to 4 MPa, Figure 8a) to foam in personal protective
 423 equipment (~1 MPa [58–60]), running shoe midsoles (~2 MPa [33,61]) liners for prosthetic
 424 sockets (~1 MPa [62]) and expanded foam in helmets (~5 to 20 MPa [63–65]). Foams
 425 fabricated herein also had a wide range of tensile moduli (5 to 12 MPa, Figure 8), similar to
 426 that of expanded foam used in helmets. These foams were up to twice as stiff as similar foam
 427 fabricated without constraints [49]. While similar stiffness open cell auxetic foams have been
 428 fabricated before [31], these closed cell auxetic foams have higher porosity (FDRs up to 5,
 429 Figure 3, than $FDR \approx 10$ in previous work [31]), and high magnitude NPR during loading in
 430 the same axes as their desirable Young's moduli (~1 to 12 MPa, Figures 7 & 8). Alignment of
 431 desirable characteristics (NPR and Young's modulus), and high porosity, mean these auxetic
 432 closed cell foams could realise the previously demonstrated [4–6,8,28,37,66] and discussed
 433 [30,67–69] benefits of NPR to energy absorption [33,51,58–60,62–65]. The presented methods
 434 facilitate further development and testing, including impact testing at different temperatures
 435 and humidities, of auxetic and gradient foam for often discussed [1,19,30,68], but unrealised,
 436 applications for auxetic foam.

437 5. Conclusions

We demonstrate control over compression and cell structure during auxetic closed cell foam fabrications. Poisson's ratios between -1 and 1, compressive tangent moduli from 1 to 4 MPa and tensile Young's moduli between 5 and 12 MPa were shown within a gradient sample. Obtained mechanical properties agree (within ~1 S.D.) with analytical models adapted from previous models for auxetic open cell and conventional closed cell foam. Open cell gradient auxetic foam is available, but typically with Young's moduli at least ten times lower than that of the closed cell foams presented here. Now that such control is possible during closed cell auxetic and gradient foam fabrications, prototype devices featuring auxetic and gradient foam, such as sporting personal protective equipment, helmets, prosthetics and footwear, can be developed and tested. Future work could impact test the foams developed here for such applications. The development of an analytical model for auxetic closed cell foam provides a better understanding of such foams, which could help in their application to sports equipment and other devices.

6. Acknowledgements

The work was funded by Manchester Metropolitan University's Strategic Opportunities Fund, and Sheffield Hallam University's Creating Knowledge Investment Platform. Characterisation, testing, writing and analysis was under taken by Dr. Duncan, with equal guidance given by both co-authors.

7. References

1. Lakes RS. Foam Structures with a Negative Poisson's Ratio. *Science* (80-). 1987.235(4792). 1038–40.
2. Cross TM, Hoffer KW, Jones DP, Kirschner PB, Meschter JC. Auxetic Structures And Footwear With Soles Having Auxetic Structures (US 2015/0075034 A1). Vol. 1. 2015.
3. Moroney C, Alderson A, Allen T, Sanami M, Venkatraman P. The Application of Auxetic Material for Protective Sports Apparel. *Proceedings*. 2018.2(6). 251.
4. Chan N, Evans KE. Indentation resilience of conventional and auxetic foams. *J Cell Plast*. 1998.34. 231–60.
5. Lakes RS, Elms K. Indentability of conventional and negative Poisson's ratio foams. *J Compos Mater*. 1993.27(12). 1193–202.
6. Ge C. A comparative study between felted and triaxial compressed polymer foams on cushion performance. *J Cell Plast*. 2013.49(6). 521–33.
7. Lisiecki J, Błazejewicz T, Kłysz S, Gmurczyk G, Reymer P, Mikułowski G. Tests of polyurethane foams with negative Poisson's ratio. *Phys Status Solidi Basic Res*. 2013.250(10).

- 1988–95.
8. Allen T, Shepherd J, Hewage TAM, Senior T, Foster L, Alderson A. Low-kinetic energy impact response of auxetic and conventional open-cell polyurethane foams. *Phys Status Solidi Basic Res.* 2015.9. 1–9.
9. Scarpa F, Ciffo LG, Yates JR. Dynamic properties of high structural integrity auxetic open cell foam. *Smart Mater Struct.* 2003.13(1). 49–56.
10. Scarpa F, Pastorino P, Garelli A, Patsias S, Ruzzene M. Auxetic compliant flexible PU foams: Static and dynamic properties. *Phys Status Solidi Basic Res.* 2005.242(3). 681–94.
11. Scarpa F, Giacomini J, Zhang Y, Pastorino P. Mechanical performance of auxetic polyurethane foam for antivibration glove applications. *Cell Polym.* 2005.24(5). 253–68.
12. Li Q, Yang D. Vibro-acoustic performance and design of annular cellular structures with graded auxetic mechanical metamaterials. *J Sound Vib [Internet].* 2020.466. 115038. Available from: <https://doi.org/10.1016/j.jsv.2019.115038>
13. Li Q, Yang D. Vibration and Sound Transmission Performance of Sandwich Panels with Uniform and Gradient Auxetic Double Arrowhead Honeycomb Cores. *Shock Vib.* 2019.2019.
14. Howell B, Prendergast P, Hansen L. Examination of acoustic behavior of negative poisson's ratio materials. *Appl Acoust.* 1994.43(2). 141–8.
15. Almutairi MM, Osman M, Tlili I. Thermal Behavior of Auxetic Honeycomb Structure: An Experimental and Modeling Investigation. *J Energy Resour Technol Trans ASME.* 2018.140(12).
16. Innocenti P, Scarpa F. Thermal conductivity properties and heat transfer analysis of Multi-re-entrant auxetic honeycomb structures. *J Compos Mater.* 2009.43(21). 2419–39.
17. Chun Checn H, Scarpa F, Hallak Panzera T, Farrow I, Peng H-X. Shear stiffness and energy absorption of auxetic open cell foams as sandwich cores. *Phys Status Solidi.* 2018.256(1). 1–9.
18. Timoshenko SP, Goodier JN. *Theory of Elasticity.* 3rd ed. New York: McGraw-Hill, USA; 1970.
19. Alderson A, Alderson KL, McDonald SA, Mottershead B, Nazare S, Withers PJ, et al. Piezomorphic materials. *Macromol Mater Eng.* 2013.298(3). 318–27.
20. Evans KE. The design of doubly curved sandwich panels with honeycomb cores. *Compos Struct.* 1991.17(2). 95–111.
21. Chan N, Evans KE. Fabrication methods for auxetic foams. *J Mater Sci.* 1997.32. 5945–53.
22. Li Y, Zeng C. Room-Temperature, Near-Instantaneous Fabrication of Auxetic Materials with Constant Poisson's Ratio over Large Deformation. *Adv Mater.* 2016.28(14). 2822–6.
23. Sanami M, Alderson A, Alderson KL, McDonald S a., Mottershead B, Withers PJ. The production and characterization of topologically and mechanically gradient open-cell thermoplastic foams. *Smart Mater Struct.* 2014.23(5). 055016.
24. Lowe A, Lakes RS. Negative Poisson's ratio foam as seat cushion material. *Cell Polym.* 2000.19(3). 157–67.
25. Stojmanovski Mercieca LA, Formosa C, Grima JN, Chockalingam N, Gatt R, Gatt A. On the Use of Auxetics in Footwear: Investigating the Effect of Padding and Padding Material on Forefoot Pressure in High Heels. *Phys Status Solidi Basic Res.* 2017.254(12). 1–5.
26. Allen T, Duncan O, Foster L, Senior T, Zampieri D, Edeh V, et al. Auxetic foam for snow-sport safety devices. *Snow Sport Trauma Saf Proc Int Soc Ski Saf.* 2016.21.
27. Foster L, Peketi P, Allen T, Senior T, Duncan O, Alderson A. Application of Auxetic Foam in Sports Helmets. *Appl Sci.* 2018.8(3). 354.
28. Duncan O, Foster L, Senior T, Alderson A, Allen T. Quasi-static characterisation and impact testing of auxetic foam for sports safety applications. *Smart Mater Struct.* 2016.25(5). 054014.
29. Critchley R, Corni I, Wharton JA, Walsh FC, Wood RJK, Stokes KR. A review of the manufacture, mechanical properties and potential applications of auxetic foams. *Phys Status Solidi Basic Res.* 2013.250(10). 1963–82.
30. Duncan O, Shepherd T, Moroney C, Foster L, Venkatraman PD, Winwood K, et al. Review of auxetic materials for sports applications: Expanding options in comfort and protection. *Appl Sci.* 2018.8(6). 941.
31. Zhang Q, Lu W, Scarpa F, Barton D, Lakes RS, Zhu Y, et al. Large stiffness thermoformed open cell foams with auxeticity. *Appl Mater Today.* 2020.20. 100775.

- 526 32. Ankrah S, Mills NJ. Analysis of ankle protection in Association football. *Sport Eng.*
527 2004.7(1). 41–52.
- 528 33. Mills NJ, Fitzgerald C, Gilchrist A, Verdejo R. Polymer foams for personal protection:
529 Cushions, shoes and helmets. *Compos Sci Technol.* 2003.63(16). 2389–400.
- 530 34. Mills NJ. The biomechanics of hip protectors. *Proc Inst Mech Eng H.* 1996.210(4). 259–66.
- 531 35. Duncan O, Clegg F, Essa A, Bell AMT, Foster L, Allen T, et al. Effects of Heat Exposure and
532 Volumetric Compression on Poisson's Ratios, Young's Moduli, and Polymeric Composition
533 During Thermo-Mechanical Conversion of Auxetic Open Cell Polyurethane Foam. *Phys*
534 *Status Solidi.* 2019.
- 535 36. Grima JN, Attard D, Gatt R. A novel process for the manufacture of auxetic foams and for the
536 conversion of auxetic foam to conventional form (WO 2010049511 A2). 2010. 1–5.
- 537 37. Lisiecki J, Klysz S, Blazejewicz T, Gmurczyk G, Reymer P. Tomographic examination of
538 auxetic polyurethane foam structures. *Phys Status Solidi Basic Res.* 2013.251(2). 314–20.
- 539 38. Alderson A, Davies PJ, Alderson KIML, Smart GM. The Effects of Processing on the
540 Topology and Mechanical Properties of Negative Poisson's Ratio Foams. *Proc IMECE2005*
541 *2005 ASME Int Mech Eng Congr Expo Proc IMECE200.* 2005. 1–8.
- 542 39. Bianchi M, Scarpa F, Banse M, Smith CW. Novel generation of auxetic open cell foams for
543 curved and arbitrary shapes. *Acta Mater.* 2011.59(2). 686–91.
- 544 40. Duncan O, Allen T, Foster L, Senior T, Alderson A. Fabrication, characterisation and
545 modelling of uniform and gradient auxetic foam sheets. *Acta Mater.* 2017.126. 426–37.
- 546 41. Gibson LJ, Ashby MF. Cellular solids. Structure and properties. **1997.** 67, 176–183, 259–264,
547 286, 301, 498 p.
- 548 42. Imam S, Driscoll H, Winwood K, Venkatraman P, Allen T. Efficacy of Density in Predicting
549 the Protective Properties of Padded Clothing in Rugby †. *Proc 13th Conf Int Sport Eng Assoc.*
550 *2020.49(38).* 1–7.
- 551 43. Mills NJ. Foam protection in sport. In: Jenkins M, editor. *Materials in sports equipment.*
552 *Volume 1.* Cambridge, UK: Woodhead Publishing Limited; **2003.** p. 20–9.
- 553 44. Mawkhlieng U, Majumdar A. Soft body armour. *Text Prog.* 2019.51(2). 139–224.
- 554 45. Sterzing T, Custozza G, Ding R, Cheung JTM. Segmented midsole hardness in the midfoot to
555 forefoot region of running shoes alters subjective perception and biomechanics during heel-toe
556 running revealing potential to enhance footwear. *Footwear Sci.* 2015.7(2). 63–79.
- 557 46. Mohsenizadeh S, Ahmad Z, Alipour R, Majid RA, Prawoto Y. Quasi Tri-Axial Method for the
558 Fabrication of Optimized Polyurethane Auxetic Foams. *Phys Status Solidi.* 2019.1800587.
559 1800587.
- 560 47. Martz EO, Lee T, Lakes RS, Goel VK, Park JB. Re-entrant transformation methods in closed
561 cell foams. *Cell Polym.* 1996.15(4). 229–49.
- 562 48. Fan D, Li M, Qiu J, Xing H, Jiang Z, Tang T. Novel Method for Preparing Auxetic Foam from
563 Closed-Cell Polymer Foam Based on the Steam Penetration and Condensation Process. *ACS*
564 *Appl Mater Interfaces.* 2018.
- 565 49. Duncan O, Birch A, Allen T, Foster L, Hart J, Alderson A. Effect of steam conversion on the
566 cellular structure, Young's modulus and negative Poisson's ratio of closed cell foam. *Smart*
567 *Mater Struct.* 2020.((Accepted)).
- 568 50. Masters IG, Evans KE. Models for the elastic deformation of honeycombs. *Compos Struct.*
569 1996.35(4). 403–22.
- 570 51. Mills NJ, Zhu HX. The high strain compression of closed-cell polymer foams. *J Mech Phys*
571 *Solids.* 1999.47(3). 669–95.
- 572 52. Rusch KC. Load-compression behavior of brittle foams. *J Appl Polym Sci.* 1970.14(5). 1263–
573 76.
- 574 53. Annual Book of ASTM Standards. Standard Test Methods for Flexible Cellular Materials —
575 Slab, Bonded, and Molded Urethane Foams. Annual Book of ASTM Standards 2008.
- 576 54. Wang D, Diazdelao FA, Wang W, Lin X, Patterson EA, Mottershead JE. Uncertainty
577 quantification in DIC with Kriging regression. *Opt Lasers Eng.* 2016.78. 182–95.
- 578 55. Mills NJ, Gilchrist A. Modelling the indentation of low density polymer foams. *Cell Polym.*
579 *2000.19(6).* 389–412.
- 580 56. Ramaswamy H. Fabrication and testing of 2-dimensional Z-expandable auxetic textile

1
2
3
4
5
6
7
8
9
10
11
12
13
14
15
16
17
18
19
20
21
22
23
24
25
26
27
28
29
30
31
32
33
34
35
36
37
38
39
40
41
42
43
44
45
46
47
48
49
50
51
52
53
54
55
56
57
58
59
60

structures for impact protective clothing applications. 2014. 1–15.

57. Allen T, Hewage T, Newton-Mann C, Wang W, Duncan O, Alderson A. Fabrication of Auxetic Foam Sheets for Sports Applications. *Phys Status Solidi Basic Res.* 2017.1700596. 1–6.

58. Signetti S, Nicotra M, Colonna M, Pugno NM. Modeling and simulation of the impact behavior of soft polymeric-foam-based back protectors for winter sports. *J Sci Med Sport.* 2018.

59. Nicotra M, Moncalero M, Messori M, Fabbri E, Fiorini M, Colonna M. Thermo-mechanical and impact properties of polymeric foams used for snow sports protective equipment. *Procedia Eng.* 2014.72. 678–83.

60. Ankrah S, Mills NJ. Performance of football shin guards for direct stud impacts. *Sport Eng.* 2003.6(4). 207–19.

61. Verdejo R, Mills NJ. Heel-shoe interactions and the durability of EVA foam running-shoe midsoles. *J Biomech.* 2004.37(9). 1379–86.

62. Sanders JE, Greve JM, Mitchell SB, Zachariah SG. Material properties of commonly-used interface materials and their static coefficients of friction with skin and socks. *J Rehabil Res Dev.* 1998.35(2). 161–76.

63. Krundaeva A, De Bruyne G, Gagliardi F, Van Paepegem W. Dynamic compressive strength and crushing properties of expanded polystyrene foam for different strain rates and different temperatures. *Polym Test.* 2016.55(2016). 61–8.

64. Mosleh Y, Bosche K Vanden, Sloten J Vander, Verpoest I, Ivens J. Combined shear-compression test to characterize foams under oblique loading for bicycle helmets. In: *Proceedings of the 16rd European Conference on Composites Materials ECCM16, Seville, Spain. 2014.* p. 22–6.

65. Andena L, Caimmi F, Leonardi L, Ghisi A, Mariani S, Braghin F. Towards Safer Helmets: Characterisation, Modelling and Monitoring. *Procedia Eng.* 2016.147. 478–83.

66. Pastorino P, Scarpa F, Patsias S, Yates JR, Haake SJ, Ruzzene M. Strain rate dependence of stiffness and Poisson’s ratio of auxetic open cell PU foams. *Phys Status Solidi Basic Res.* 2007.244(3). 955–65.

67. Novak N, Vesenjask M, Ren Z. Auxetic cellular materials - A review. *Stroj Vestnik/Journal Mech Eng.* 2016.62(9). 485–93.

68. Evans KE, Alderson A. Auxetic materials: Functional materials and structures from lateral thinking! *Adv Mater.* 2000.12(9). 617–28.

69. Yang W, Li ZM, Shi W, Xie BH, Yang MB. On auxetic materials. *J Mater Sci.* 2004.39(10). 3269–79.